Memoirs of the Faculty of Engineering, Okayama University, Vol. 45, pp. 1-14, January 2011

Optimal Digital Control Systems Design for Handling Machines using dsPIC

Tatsuro AKIYOSHI * , Jun IMAI and Masami KONISHI
Dept. of Electrical and Electronic Engineering
Okayama University
3-1-1, Tsushima-Naka Okayama, 700-8530

(Received December 24, 2010)

This paper presents a method of the controller design for the handling machine by using dsPIC(Digital Signal Processor + Peripheral Interface Controller). Recently, many manufacturing robots are operated in manufacturing facilities, with the aim of labor, cost saving, and improvement of the productivity. Such robots need to have positioning performance of high precision and simultaneously to save cost. In this paper, a digital optimal servo controller is designed, and it is implemented into our barebones controller which involves dsPIC. We have designed and manufactured the controller which is added suitable peripherals to improve the consistency between the mechanical machine operating in continuous time and controller in discrete time. The significance of this research is that digital implementation of the embedded system which has performance-limitation has ensured a comparable result, against the one with PC which has broad utility. When it is used as a controller, it is possible to restrain product prices greatly equivalent PC precision. We demonstrate potential that good control can be achieved even with low cost. Our research has lead to the viability of lower cost and higher performance system for the production process at factories.

1 INTRODUCTION

In the industrial world, it is in the trend of low cost and energy saving, and industrial robots are required positioning control for productivity improvement and saving of energy. In other words, industrial robots in production field are required in fast and smooth behavior, and low cost of industrial robots main and the system for controlling are desired. Furthermore, the power consumption at the time of robot operation should be small for industrial current needs.

In this paper, the controlled plant is a robot arm which is driven by direct-drive (DD) motor with single-degree-of-freedom that simulates the wafer handling device in semiconductor plant as an electromechanical system. DD motor is expected to be small size and to have precise position control, and is desired to use for robot device systems. Moreover, it can remove the factors of tracking error, resonance, and other deterioration effects, because it excels in the rigidity and the performance of disturbance rejection compared with conventional systems. We can obtain equal results to control by using PC even if we design the embedded system controller which does not consider stiffness and disturbance.

This paper reports the results of applying the embedded system that is designed and produced and is involved mainly dsPIC, which is a part of microcomputer, as a CPU. The embedded system means that it limits to a specific function. The significance of this research is that digital implementation of the embed-

*E-mail: en18402@s.okadai.jp

ded system which has performance-limited, against PC which has broad utility, has ensured a good result. If this embedded system can be used as a controller, it will be able to work equivalent accuracy and depress a price considerably against PC. This achieves high performance and low cost that is trend of the industrial world in recent years. The development process can be done by the consistent technique, and it also leads to improve the productivity of the embedded system controller in another field, if the controlled plant can be controlled excellently in this research.

The rest of the paper is as follows Section 2 presents the outlines of the wafer handling machine, and the controller hardware. Section 3 presents that the state eq. of controlled plant is led by using Lagrange eq. of motion. The nonlinear term is included in obtained model, however, the linearization is done to a nonlinear for designing easily. Section 4 presents that the integral type of optimal servo system is composed on transfer function obtained in Section 3. The optimal regulator is designed to decide the best gain. This is designed that the control input is small, and do well to track with the target value. Section 5 presents that the embedded system is designed and produced in consideration of the consistency between the controller and DD motor which is the driving source of the wafer handling machine. It is simulated to the control machine. Finally, the produced controller is applied to the real machine, and considering it. Section 6 presents conclusion.

2 THE HANDLING MACHINE AND CONTROLLER

This section presents the outline of the wafer handling machine and the controller.

2.1 The Components and Function of The Handling Machine

The wafer handling machine as a controlled plant is shown in Fig.1. The arm that puts a wafer, it connects directly with DD(Direct Drive) motor, the joint between DD motor and the arm is fixed. DD motor works in connection with the movement of the arm. DD motor is simple structure and low cost of supplies, and is expected to work smoother, even without decelerator, than the motor which is included a decelerator. Moreover, it can remove the factors of tracking error,

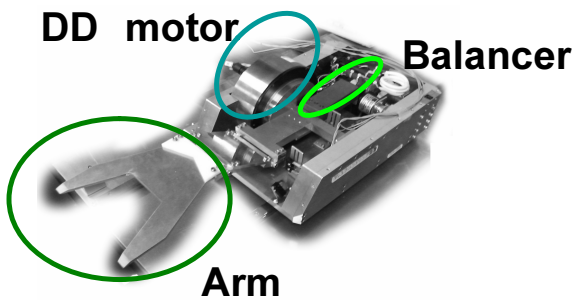

Fig. 1 The handling machine

resonance, and other deterioration effects in servo, because it excels in the rigidity and the performance of disturbance rejection compared with a current servo system. The balancer is assembled for keeping balance in the arm. The object operation in this paper is a vertical work of the arm. DD motor ratings and specifications are shown in Appendix A.

2.2 The Hardware Outline of The Controller

This paper does not use a PC for controlling. The controller is embedded system which puts the microcomputer on CPU. The dsPIC (Digital Signal Controller + Peripheral Interface Controller) is 16 bits microcomputer with DSP supplied by the microchip Inc. Fig.2 shows the appearance of dsPIC. The dsPIC30F4011 is selected among the motor control series because it has the sufficient internal modules. Refer to Appendix B for details.

Fig. 2 An appearance of dsPIC

3 MATHEMATICAL MODELING FOR THE MACHINE

This section presents to develop for mathematical model by using modern control theory[3], and shows the state space model.

3.1 Modeling for Handling Machine

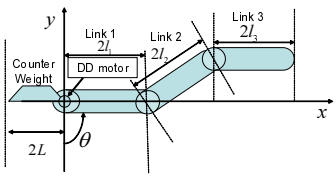

Fig. 3 The component of the handling machine

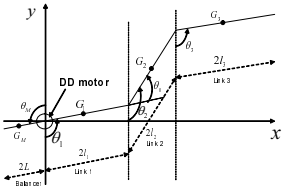

Fig. 4 The model of handling machine

Fig.3 shows the components of the handling machine, and Fig.4 shows the model of the handling machine. The physics parameter referred to Appendix C for details. The barycentric coordinate of each links become the eqs.(1)-(8) from Fig.4. (x_1, y_1), (x_2, y_2), (x_3, y_3) , (X, Y) are the barycentric coordinate of link1, link2, link3, and the counter weight, respectively.

$$x_1 = l_1 \sin\theta_1, \tag{1}$$
$$y_1 = -l_1 \cos\theta_1, \tag{2}$$
$$x_2 = 2l_1 \sin\theta_1 + l_2 \sin\theta_2, \tag{3}$$
$$y_2 = -2l_1 \cos\theta_1 - l_2 \cos\theta_2, \tag{4}$$
$$x_3 = 2l_1 \sin\theta_1 + 2l_2 \sin\theta_2 + l_3 \sin\theta_3, \tag{5}$$
$$y_3 = -2l_1 \cos\theta_1 - l_2 \cos\theta_2 - l_3 \cos\theta_3, \tag{6}$$
$$X = -L \sin\theta_M, \tag{7}$$
$$Y = L \cos\theta_M. \tag{8}$$

The moment of inertia [4] I_1, I_2, I_3 of link 1,2,3 are obtained in Fig.4. These are shown in eq.(9)-(14). I_{Gx} means the moment of inertia about the center of rotation in link x.

$$I_{G1} = \frac{m_1}{2l_1}\int_{-l_1\sin\theta_1}^{l_1\sin\theta_1} r_1^2 dr_1 = \frac{1}{3}m_1 l_1^2 \sin^2\theta_1, \tag{9}$$
$$I_1 = I_{G1} + m_1(l_1\sin\theta_1)^2 = \frac{3}{4}m_1 l_1^2 \sin^2\theta_1, \tag{10}$$
$$I_{G2} = \frac{m_2}{2l_2}\int_{-l_2\sin\theta_2}^{l_2\sin\theta_2} r_2^2 dr_2 = \frac{1}{3}m_2 l_2^2 \sin^2\theta_2, \tag{11}$$
$$\begin{aligned} I_2 &= I_{G2} + (m_1+m_2)(2l_1\sin\theta_1 + l_2\sin\theta_1)^2 \\ &= \frac{4}{3}m_2 l_2^2\sin^2\theta_2 + 4m_1 l_1^2\sin^2\theta_1 \\ &\quad +4m_2 l_1^2\sin^2\theta_1 + m_1 l_2^2\sin^2\theta_2 \\ &\quad +4(m_1+m_2)l_1 l_2 \sin\theta_1\sin\theta_2, \end{aligned} \tag{12}$$
$$I_{G3} = \frac{m_3}{2l_3}\int_{-l_3\sin\theta_3}^{l_3\sin\theta_3} r_3^2 dr_3 = \frac{1}{3}m_3 l_3^2\sin^2\theta_3, \tag{13}$$
$$\begin{aligned} I_3 &= I_{G3} + (m_1+m_2+m_3) \\ &\quad (2l_1\sin\theta_1 + 2l_2\sin\theta_2 + l_3\sin\theta_3)^2 \\ &= \frac{4}{3}m_3 l_3^2\sin^2\theta_3 + 4m_1 l_1^2\sin^2\theta_1 \\ &\quad +4m_2 l_2^2\sin^2\theta_2 + 4(m_2+m_3)l_1^2\sin^2\theta_1 \\ &\quad +4(m_1+m_3)l_2^2\sin^2\theta_2 + (m_1+m_2)l_3^2\sin^2\theta_3 \\ &\quad +8(m_1+m_2+m_3)l_1 l_2\sin\theta_1\sin\theta_2 \\ &\quad +4(m_1+m_2+m_3)l_1 l_3\sin\theta_1\sin\theta_3 \\ &\quad +4(m_1+m_2+m_3)l_2 l_3\sin\theta_2\sin\theta_3. \end{aligned} \tag{14}$$

The inertia moment of between link and DD motor is set to J in Fig.4, so the movement energy function T is solved as follows:

$$\begin{aligned} T &= \frac{1}{2}m_1(\dot{x}_1^2+\dot{y}_1^2) + \frac{1}{2}I_1\dot{\theta}_1^2 + \frac{1}{2}m_2(\dot{x}_2^2+\dot{y}_2^2) \\ &\quad +\frac{1}{2}I_2\dot{\theta}_2^2 + \frac{1}{2}m_3(\dot{x}_3^2+\dot{y}_3^2) + \frac{1}{2}I_3\dot{\theta}_3^2 \\ &\quad +\frac{1}{2}M(\dot{X}^2+\dot{Y}^2) + \frac{1}{2}I_c\dot{\theta}_M^2 + \frac{1}{2}J\dot{\theta}_1^2. \end{aligned} \tag{15}$$

It is known as $\theta_1 = \theta_M = \theta_3$,$\theta_2 = \theta_0 + \theta_1$ in Fig.4, and set up $\theta = \theta_1$. By substituting the eqs. (1)-(8) into the eq. (15), we obtain

$$\begin{aligned} T &= \frac{1}{2}\dot{\theta}^2[m_1 l_1^2 + m_2(4l_1^2 + l_2^2 + 4l_1 l_2\cos\theta_0) \\ &\quad +m_3(4l_1^2 + 4l_2^2 + l_3^2 + 8l_1 l_2\cos\theta_0 + 4l_2 l_3\cos\theta_0 \\ &\quad +4l_1 l_3) + I_1 + I_2 + I_3 + I_c + J + ML^2]. \end{aligned} \tag{16}$$

The potential energy function U shows as follows:

$$U = m_1 g y_1 + m_2 g y_2 + m_3 g y_3 + MgY. \tag{17}$$

The eq.(18) shows dissipative energy function D, and the viscous friction coefficient of shaft is $\hat{c}$.

$$D = \frac{1}{2}\hat{c}\dot{\theta}^2. \tag{18}$$

The eq.(19) shows the Lagrange equation of motion, and $\tau(t)$ means torque input.

$$\tau(t) = \frac{d}{dt}\left(\frac{\partial T}{\partial \dot{\theta}}\right) - \frac{\partial T}{\partial \theta} + \frac{\partial D}{\partial \dot{\theta}} + \frac{\partial U}{\partial \theta}. \tag{19}$$

By substituting the eqs.(16)-(18) into (19), we obtain,

$$a\ddot{\theta}(t) = -b\sin\theta(t) - e\cos\theta(t) - \hat{c}\dot{\theta}(t) + \tau(t). \tag{20}$$

a, b, and e are shown as follows:

$$\begin{aligned} a &= m_1 l_1^2 + m_2(4l_1^2 + l_2^2 + 4l_1 l_2\cos\theta_0) \\ &\quad + m_3(4l_1^2 + 4l_2^2 + l_3^2 + 8l_1 l_2\cos\theta_0 + 4l_2 l_3\cos\theta_0 \\ &\quad + 4l_1 l_3) + ML^2 + I_1 + I_2 + I_3 + I_c + J, \end{aligned} \tag{21}$$

$$\begin{aligned} b &= g[m_1 l_1 + m_2(2l_1 + \frac{\sqrt{2}}{2}l_2) \\ &\quad + m_3(2l_1 + \sqrt{2}l_2 + l_3) - ML], \end{aligned} \tag{22}$$

$$e = g(\frac{1}{\sqrt{2}}m_2 l_2 + \sqrt{2}m_3 l_2). \tag{23}$$

3.2 Linearized State Equation

It is difficult to design controller because the eq. (20) is included nonlinear term. The state eq. is led by linearizing with Taylor expansion in the operating point. It linearizes with Taylor expansion in $\theta = \pi/2(= \bar{\theta})$ in Fig.4. It is substituted $\theta = \pi/2$ into the eq.(20).

$$\bar{\tau} = b. \tag{24}$$

The small variation of the arm angle and input torque is defined as $\Delta\theta(t)$ and $\Delta\tau(t)$, respectively as follows:

$$\theta(t) = \bar{\theta} + \Delta\theta(t), \tag{25}$$

$$\tau(t) = \bar{\tau} + \Delta\tau(t). \tag{26}$$

eqs.(24)-(26) are substituted into the eq.(20) and we obtain

$$\begin{aligned} a\frac{d^2}{dt^2}(\frac{\pi}{2} + \Delta\theta) &= -b\sin(\frac{\pi}{2} + \Delta\theta) - e\cos(\frac{\pi}{2} + \Delta\theta) \\ &\quad -\hat{c}\frac{d}{dt}(\frac{\pi}{2} + \Delta\theta) + (\bar{\tau} + \Delta\tau), \end{aligned} \tag{27}$$

$$\begin{aligned} \Delta\ddot{\theta}(t) &= -\frac{b}{a}\cos\Delta\theta(t) + \frac{e}{a}\sin\Delta\theta(t) \\ &\quad -\frac{c}{a}\Delta\dot{\theta}(t) + \frac{1}{a}\Delta\tau(t) + \frac{b}{a}. \end{aligned} \tag{28}$$

Using the 1st terms of Taylor expansion around $\theta = \pi/2$ of $\cos\Delta\theta(t) and \sin\Delta\theta(t)$

$$\cos\Delta\theta(t) \approx 1, \tag{29}$$

$$\sin\Delta\theta(t) \approx \Delta\theta. \tag{30}$$

Eqs. (29) and (30) are substituted into eq.(28), we obtain

$$\begin{aligned} \Delta\ddot{\theta}(t) &= -\frac{b}{a} + \frac{e}{a}\Delta\theta(t) - \frac{c}{a}\Delta\dot{\theta}(t) + \frac{1}{a}\Delta\tau(t) + \frac{b}{a} \\ &= \frac{e}{a}\Delta\theta - \frac{c}{a}\Delta\dot{\theta}(t) + \frac{1}{a}\Delta\tau(t), \end{aligned} \tag{31}$$

and this is rewritten as a state space model:

$$\begin{bmatrix} \Delta\dot{\theta} \\ \Delta\ddot{\theta} \end{bmatrix} = \begin{bmatrix} 0 & 1 \\ \frac{e}{a} & -\frac{c}{a} \end{bmatrix} \begin{bmatrix} \Delta\theta \\ \Delta\dot{\theta} \end{bmatrix} + \begin{bmatrix} 0 \\ \frac{1}{a} \end{bmatrix} \Delta\tau(t). \tag{32}$$

Here, we define $x = \begin{bmatrix} \Delta\theta \\ \Delta\dot{\theta} \end{bmatrix}$, $y(t) = \Delta\theta(t)$,

$A = \begin{bmatrix} 0 & 1 \\ \frac{e}{a} & -\frac{c}{a} \end{bmatrix}$, and $B = \begin{bmatrix} 0 \\ \frac{1}{a} \end{bmatrix}$.

A state equation is written as

$$\dot{x} = Ax(t) + B\Delta\tau(t). \tag{33}$$

We also define $C = [1 \quad 0]$,

and output equation is

$$y = Cx(t). \tag{34}$$

Transforming the eq.(31), we obtain

$$\Delta\theta(t) = \frac{1}{as^2 + cs - e}\Delta\tau(t). \tag{35}$$

Therefore, eq.(36) shows a loop transfer function.

$$G(s) = \frac{1}{as^2 + cs - e}. \tag{36}$$

In Fig.5 we see the block diagram of controlled plant.

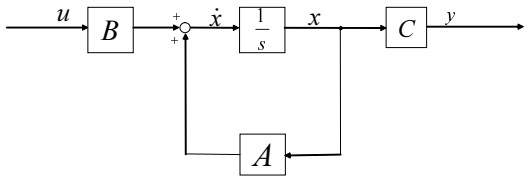

Fig. 5 The block diagram of controlled plant

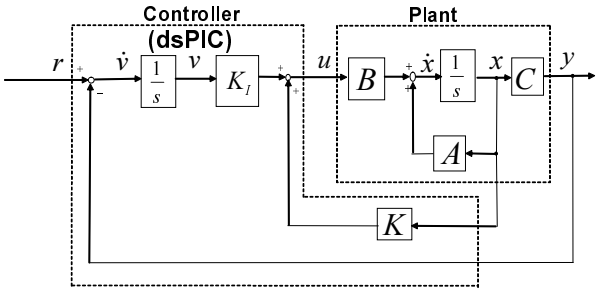

Fig. 6 The integral type of optimal system

4 THE INTEGRAL TYPE OPTIMAL SERVO SYSTEM

In this section, an integral type of optimal servo control systems[6] is designed to track well for some target value.

4.1 Outline of the Integral Type Optimal Control System

The relation between input and output of the system is illustrated in Fig.5. The target value is step function or square wave. It is assumed that the target value is step function $T(t) = n(t \geq 0)$. Laplace transform of T is $T(s) = n/s$. It can be calculated what steady-state error remains by using final value theorem in the function.

$$\begin{aligned} E(s) &= \frac{1}{1+G(s)}T(s) \\ &= \frac{ans^2+cns-en}{as^3+cs^2+(1-e)s}. \end{aligned} \tag{37}$$

Applying final value theorem to eq.(37), we obtain

$$\begin{aligned} \varepsilon &= \lim_{s\to 0} sE(s) \\ &= \lim_{s\to 0} \frac{ans^3+cns^2-ens}{as^3+cs^2+(1-e)s} = n. \end{aligned} \tag{38}$$

Eq.(38) shows that steady-state error is arisen in this handling machine. The controller with the integrator is designed for eliminating the error. Fig.6 shows that the integral type of optimal control servo system is consisted of an optimal regulator and the integrator.

Eqs.(39)-(41) are led from Fig.6 as follows:

$$u(t) = Kx(t) + K_I v(t), \tag{39}$$

$$v(t) = \int_0^t \dot{v}(t)dt, \tag{40}$$

$$\dot{v}(t) = r - y(t). \tag{41}$$

An extended model with new state variable $x_e(t) = [x(t) \quad v(t)]^T$ is denoted as follows:

$$\begin{aligned} \begin{bmatrix} \dot{x}(t) \\ \dot{v}(t) \end{bmatrix} &= \begin{bmatrix} A & 0 \\ -C & 0 \end{bmatrix} \begin{bmatrix} x(t) \\ v(t) \end{bmatrix} \\ &\quad + \begin{bmatrix} B \\ 0 \end{bmatrix} u(t) + \begin{bmatrix} 0 \\ 1 \end{bmatrix} r, \\ \dot{x}_e(t) &= A_e x_e(t) + B_e u(t) + \begin{bmatrix} 0 \\ 1 \end{bmatrix} r. \end{aligned} \tag{42}$$

x_∞, u_∞, and v_∞ is steady-state value of $x(t)$, $u(t)$, and $v(t)$, respectively. r is the target value $y(t)$. In steady state,

$$\begin{aligned} \begin{bmatrix} 0 \\ 0 \end{bmatrix} &= \begin{bmatrix} A & 0 \\ -C & 0 \end{bmatrix} \begin{bmatrix} x_\infty \\ v_\infty \end{bmatrix} \\ &\quad + \begin{bmatrix} B \\ 0 \end{bmatrix} u_\infty + \begin{bmatrix} 0 \\ 1 \end{bmatrix} r, \\ 0 &= A_e x_{e\infty} + B_e u_\infty + \begin{bmatrix} 0 \\ 1 \end{bmatrix} r. \end{aligned} \tag{43}$$

We define $\tilde{x}(t) = x(t) - x_\infty$, $\tilde{v}(t) = v(t) - v_\infty$, and $\tilde{u}(t) = u(t) - u_\infty$. The deviation $\dot{v}$ is written as follows:

$$\begin{aligned} \dot{v} &= r - Cx \\ &= Cx_\infty - Cx(\because eq.(43)) \\ &= -C\tilde{x} \to 0 \quad (t \to \infty). \end{aligned} \tag{44}$$

We see that the steady-state error in eq.(38) is eliminated in eq.(44). From eqs.(41) and (43),

$$\dot{\tilde{x}}_e(t) = A_e \tilde{x}_e(t) + B_e \tilde{u}(t) \tag{45}$$

where $A_e = \begin{bmatrix} A & 0 \\ -C & 0 \end{bmatrix}$, $B_e = \begin{bmatrix} B \\ 0 \end{bmatrix}$, and $\tilde{x}_e(t) = \begin{bmatrix} \tilde{x}(t) \\ \tilde{v}(t) \end{bmatrix}$.

From eq.(39),

$$\tilde{u}(t) = K\tilde{x}(t) + K_I\tilde{v}(t) = K_e\tilde{x}_e, \quad (46)$$

$$K_e = [K_1 \quad K_2 \quad K_I]. \quad (47)$$

Therefore, just we have to determine eq.(47). K_e is determined in next chapter by using the optimal regulator which is written closely in Appendix E.

4.2 The Feedback Gain

Here a performance index is defined as

$$J = \int_0^\infty [x^T Q x + u^T R u]dt \quad (48)$$

where

$$Q = \begin{bmatrix} q_{11} & 0 & 0 \\ 0 & q_{22} & 0 \\ 0 & 0 & q_{33} \end{bmatrix}, R = r. \quad (49)$$

We choose suitable Q and R to determine K_1, K_2, and K_I, and these are substituted into eq.(46), and we simulate them by using MATLAB/SIMULINK. The weighting matrix Q is positive-semi definite and symmetric matrix of 3×3. R is positive definite of 1×1. The details of eq.(48) are shown in Appendix E. q_{11} is the weight of angle, q_{22} is of the angular velocity, and q_{33} the torque input.

Condition 1

We assume that the weighting matrices are

$$Q = \begin{bmatrix} 5 & 0 & 0 \\ 0 & 5 & 0 \\ 0 & 0 & 5 \end{bmatrix} \text{ and } R = 1.$$

Then, $K_1 = 3.98071$, $K_2 = 2.30554$, and $K_I = 2.23607$.

Fig.7 and 8 show the simulation results.

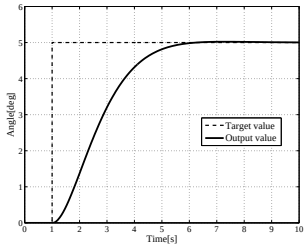

Fig. 7 Simulation result in *condition*1

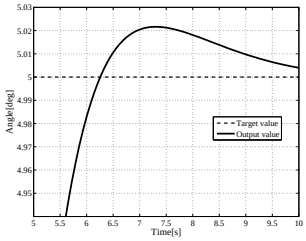

Fig. 8 A details of Fig.7 around the overshoot

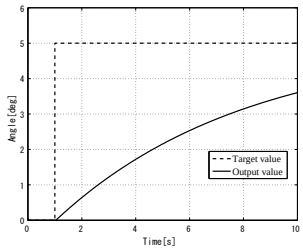

Fig. 9 Simulation result in *condition*2

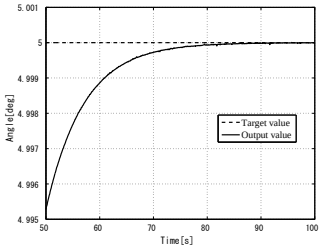

Fig. 10 The convergent point of Fig.9

We can see the overshoot by setting up the weights. This result is not satisfactory for carrying a wafer safely. Fig.7 shows the settling time that is about 4.2[s]. This is not satisfactory for production efficiency.

Condition2

We are afraid of breaking wafer because the direction of operation changes suddenly when there exists overshoot like as in the *condition*1. We define that the weight of the angle is 10000, of angle velocity is 0.01, and of torque input is 200 in *condition*2. The weight of the angle velocity is reduced more than the other two elements to make small overshoot, that is,

$$Q = \begin{bmatrix} 10000 & 0 & 0 \\ 0 & 0.01 & 0 \\ 0 & 0 & 200 \end{bmatrix} \text{ and } R = 1.$$

Then, $K_1 = 100.4689$, $K_2 = 3.8496$, and $K_I = 14.1421$.

Fig.9 and 10 show the simulation results.

We find no overshoot from Fig.10 in *condition*2. Therefore, this behavior of the arm is safer than the one of *condition*1. But, the settling time is about 85[s], so this system is nonproductive. At these results, *condition*3 has to leave the safety behavior like *condition*2 and needs to move fast like *condition*1.

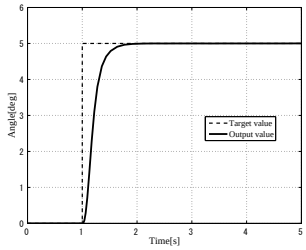

Fig. 11 Simulation result in *condition*3

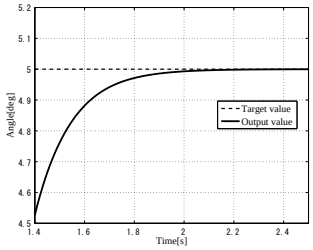

Fig. 12 The convergent point of Fig.11

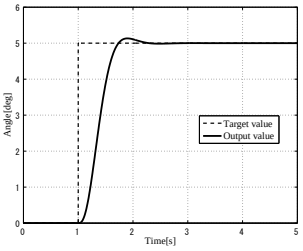

Fig. 13 Simulation result in *condition*4

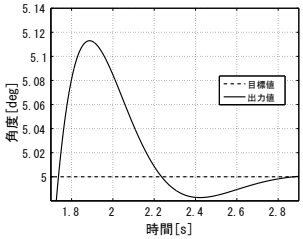

Fig. 14 The overshoot of Fig.13

*Condition*3

We define that the weight of the angle is 200, of angle velocity is 0.01, and of torque input is 10000 in *condition*3. The weight of the torque input is bigger than the weight of the angle to move fast like in *condition*2. We take

$$Q = \begin{bmatrix} 200 & 0 & 0 \\ 0 & 0.01 & 0 \\ 0 & 0 & 10000 \end{bmatrix} \text{ and } R = 1.$$

Then, $K_1 = 21.6348$, $K_2 = 1.3246$, and $K_I = 100$.

Fig.11 and Fig.12 show the simulation results.

It takes about 1[s] to converge for the target value in Fig.11. In Fig.12 we find no overshoot. We discuss whether higher performance be possible in *condition*4.

*Condition*4

We define the weight of the angle is 200, of angle velocity is 0.01, of torque input is 10000, and of R is 100 which is bigger than a current setting in *condition*4. We take

$$Q = \begin{bmatrix} 200 & 0 & 0 \\ 0 & 0.01 & 0 \\ 0 & 0 & 10000 \end{bmatrix} \text{ and } R = 100.$$

Then, $K_1 = 3.6860$, $K_2 = 0.5535$, and $K_I = 10$.

Fig.13 and Fig.14 show as the simulation results.

Fig.14 shows a overshoot around 1.7[s] and it takes 2[s] until settling. It is thought this cause is to have enlarged weight of the operation amount R=100.

Therefore, reducing the weight of control input and angle velocity and enlarging the weight ration of torque input will operate ideal to the wafer handling machine. From these results, the *condition*3 is ideal, and the feedback gain which is obtained there applies to Fig.6, that is the most suitable for the integral type optimal control system.

5 THE EMBEDDED SYSTEM WITH dsPIC

This section shows the design and production of control machine which contains dsPIC[7][8]. At first, the systematic method is shown in development of dePIC. Next, a circuit is designed which considered a consistency. Furthermore, it verifies, by the computer simulation, to confirm whether the arm is operated excellently with the designed embedded system. Finally, the produced controller applies to the real machine, and the results are considered.

5.1 The Outline of Embedded System

The outline of the system is presented in Fig.15.

Rotating angle make a pulse output from the DD motor in Fig.15. The dsPIC counts pulses, and exchange to angle. It feeds back based on the integral type optimal control servo system, and the control input is output to external DA converter. The digital value which is the arithmetic control result in dsPIC is converted into an analog value by DA converter. It is input to the motor servo pack as a voltage command. It is converted into torque in the servo pack. It is input to the DD motor as a torque command.

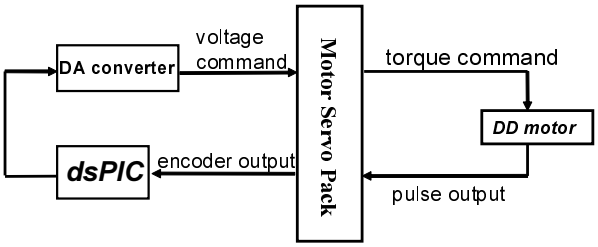

Fig. 15 System block diagram

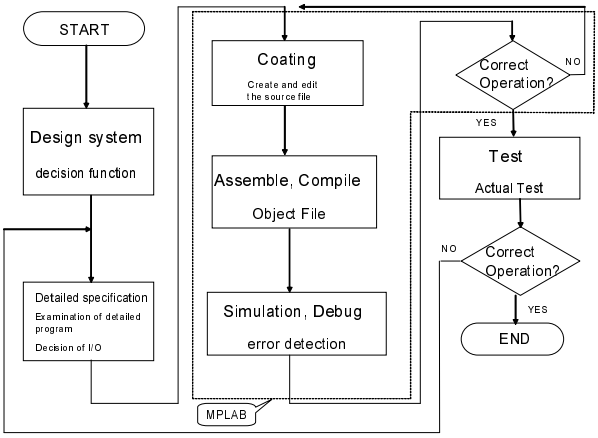

Fig. 16 Flowchart by MPLAB

5.2 Implementation of The Controller with dsPIC

Fig.16 shows the flowchart in developing of dsPIC.

The developing environment is free software MPLAB IDE(Integrated Development Environment). MPLAB C30 was used as C compiler, not used the assembly language, on MPLAB. This is because that C language is comprehensible for everyone, and agrees with a present trend as a development language than the assembly language. In order of program development, it makes calculator of program on MPLAB. If it is possible to make a program, it compiles, and debugs it. MPLAB-ICD2(In Circuit Debugger)[9] is used as a debug. The program is verified by this debugger. If bugs of program are eliminated, it is made a program file. If it is written in dsPIC by using our dsPIC writer, the program is buried in dsPIC. Finally, it applies to the real machine, and judges whether operation is normal.

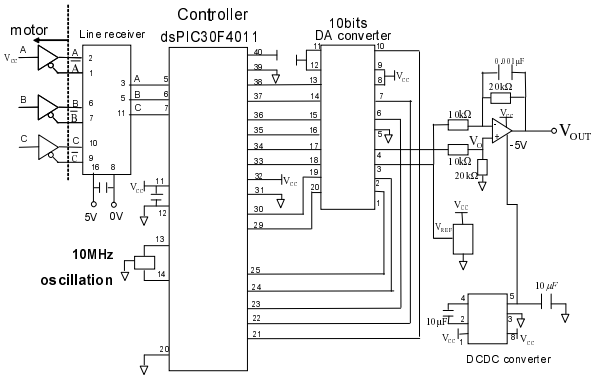

Fig. 17 The circuit diagram of the controller

5.3 Circuit Design Consistent with Handling Machine

Fig.17 shows the circuit diagram of our controller. The program is written in dsPIC according to the procedure in pervious chapter. The design is most concerned about effective utilization of program on dsPIC, but it is taken some peripherals in the difficult parts for the realization only software.

Some pulses as angle information of DD motor are input into the servo pack through the encoder. The output line-driver has generated the A, $\bar{A}$, B, $\bar{B}$, C, and $\bar{C}$ phases. A potential difference has gotten through the line-receiver and convert them into A, B and C phase, so 5[V] pulses are input into dsPIC. The pulses are counted in dsPIC, it converts them into angle in programmed calculation. The results, which are calculated from angle of rotation of DD motor, output as a digital value into DA converter. Time in dsPIC is counted by the 10[MHz] oscillation which is connected with 13,14 pin. The DA converter converts a digital value into an analog value. However, the DA converter is 10bits and unipolarity. If this goes on, DD motor rotates only one direction. The differential operation amplification is used for rotating both directions, it transforms the voltage 0-5[V] into -5[V]-+5[V]. Here, DC-DC converter transforms the voltage +5[V] into -5[V], and it is input in the operation amplification. The differential operation amplification's details denote Appendix G. The dsPIC has a high-speed motion, so a lot of currents flow to the power supply. It is designed to prevent the glitch or noises by using some bypass capacitors(0.1 μ F). Other peripherals are described in Appendix G. Fig.18 shows the controller. It is possible

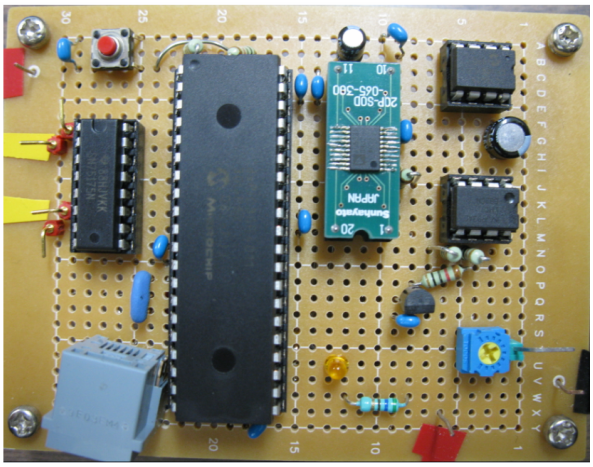

Fig. 18 The product controller

to write and debug by connecting MPLAB ICD2 with modular jack under the left. The switch upper left is set up for emergency stop.

5.4 Simulation

The target action is go up and down from -5[deg] to +5[deg]. Fig.19 shows the result of simulation. Fig.20 shows the expand of Fig.19 to observe more closely to track the target.

It takes about 1[s] to track to the target value without overshoot and steady state error in Fig.19. The digital implementation is confirmed in Fig.20. Even if dsPIC is used for the controller, it is understood to track to the target value excellently.

5.5 The Result of Implementation

In this chapter, it applies the controller to the real wafer handling machine. The target action is go up and down from -5[deg] to $+5$[deg]. The controlled period is 10[ms]. The measurement time is 20[s]. Fig.21 shows the result of implementation.

It is known to exist 0.22[deg] overshoot from Fig.22. It aims to reduce the overshoot confirmed in Fig.21, and it changes to the *system*2 that is suppressed the output value in dsPIC program against *system*1 of Fig.21. Fig.23 shows the result.

The *system*2 can be known that the measure of the overshoot is smaller than the *system*1 by comparing Fig.22 and Fig.24. The time settled to the target value after overshoot is about 0.09[s] in Fig.22, whereas it takes about 0.08[s] in Fig.24. The settling time in *system*2 is shorter than *system*1. The rising behavior of *system*1 and 2 are shown in Fig.25 and Fig.26, respectively.

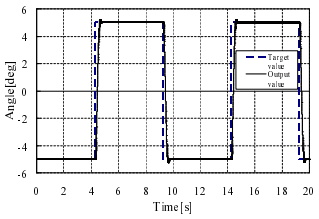

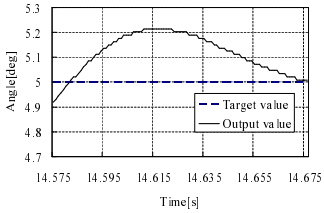

Fig. 21 The behavior of the arm (*system*1)

Fig. 22 A detail of the overshoot

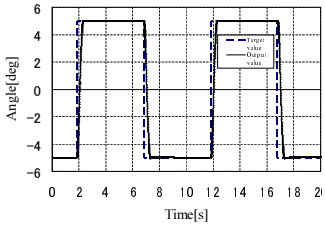

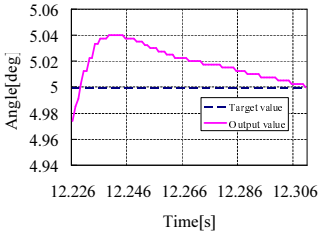

Fig. 23 The behavior of the arm (*system*2)

Fig. 24 A detail of Fig.23

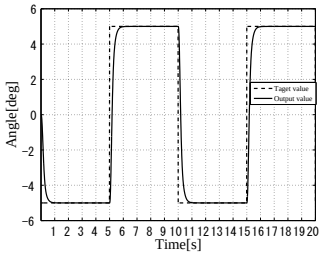

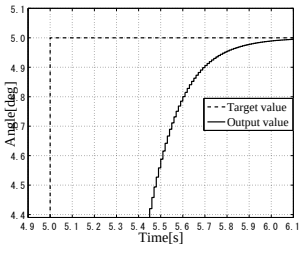

Fig. 19 Simulation result with dsPIC

Fig. 20 A detail of Fig.19

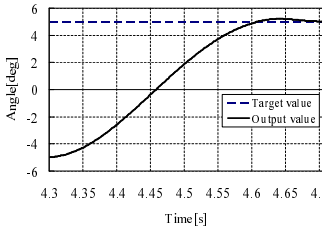

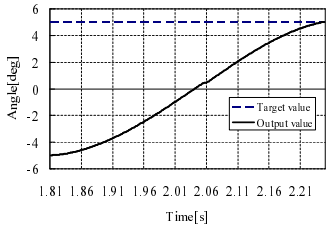

Fig. 25 Rising in *system*1

Fig. 26 Rising in *system*2

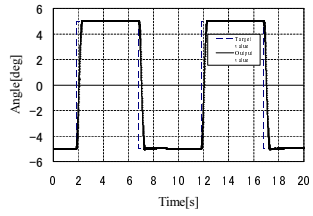

Fig. 27 The result of embedded system

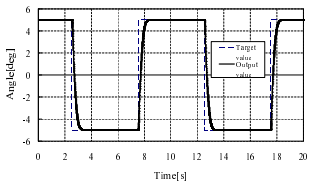

Fig. 28 The result of PC

Comparing the two systems of rising time, the settling time in Fig.25 is about 0.4[s]. The settling time of *system*2 in Fig.26 is about 0.42[s], but there exists an overshoot that cannot be confirmed in Fig.26. We see that the *system*2 settles to the target value about 0.5[s], considering the convergence time of the overshoot. Therefore, the *system*1 takes 80 % of the *system*2 in the settling time to the target value, but the *system*2 is suppressed about 80 % about the overshoot as compared with the *system*1. The *system*2 is suitable system for the handling machine because the safe carrying and excellent operation are achieved. Fig.27 and Fig.28 show the result of *system*2 and controlled by using PC, respectively.

Fig.27 and Fig.28 show that the behavior in PC is smoother around the target value. This is because the control with PC is able to calculate high-accuracy and the sampling period is small. It means that the update time of the control input is short. The advantage of embedded system with dsPIC is tracked excellently in Fig.27. The overshoot is minute, and when productivity is valued, it can be expected twice as productive as the controller with PC. In this research, when smoother operation is needed in embedded system, it is expected to improve by reviewing the control theory. Therefore, it is thought that there is room for improvement to make it to an excellent embedded controller more than now.

6 CONCLUSIONS

In this paper, so far the wafer handling machine was used as a control plant, and the embedded system was designed and produced for control. We aimed at the realization of lower cost and higher performance system with low performance device. First, the mathematics model was led from the physical perspective in the controlled plant, and the state equation was led by Lagrange's motion equation. Next, the controller was designed by using state equation based on the optimal regulator theory. This controller was insufficient as a servo system because steady state error exists. The controller with a integrator is designed for eliminating the error. The state feedback gain was determined by the performance index, the integral type optimal servo system was designed. A C-code source was written it for dsPIC, improved consistency to the controller with DD motor by using some peripherals. The embedded system was designed and produced. It was confirmed to track to the target value excellently without any overshoot and the steady state error through simulation. The produced controller was implemented to the real machine, to prove the result of simulation. The future challenge is to design a model that can take digital factors into account through sampled-data theory. We will be able to use other computer as a part of the controller which is cheaper performance and lower cost.

REFERENCES

[1] Mitchell Weiss : Semiconductor Factory Automation, pp.89-96, Solid State Technology(1996)

[2] Koichi Nakano : Position Control of Handling Machine Considering High-order Vibration Mode, Special Research Report Dept, of Electrical and Electronic Engineering Faculty of Engineering Okayama University (2008)

[3] Masatake Shiraishi : Introductory Control theory, pp.81-108, Nikkan Kogyo Shimbun,Ltd(2008)

[4] Feynman, Leighton, Sands : The Feynman Lectures on Physics1, pp.249-272, Iwanami paperback library(1998)

[5] Tomohide Naniwa : System Control with Octave/Matlab, pp.1-36, science technology publication(2000)

[6] Masakatsu Kawata, Katsuhiro Nishioka : Control Engineering with MATLAB/Simulink, pp.172-176, Morikita publication(2008)

[7] Tetsuya Gokan : Guide Book of dsPIC for Electrical Control and Signal Process , Gijyutsu Hyouronn-sya(2007)

[8] MICROCHIP : dsPIC30F4011/4012 DataSheet, pp.1-91, (2005)

[9] MICROCHIP : MPLAB ICD2 In-Debugger User's Guide, (2005)

[10] MICROCHIP : dsPIC30F Programmer's Reference Manual, (2003)

[11] ANALOG DEVICES : 2.5Vto5.5V, Parallel Interface Signal Voltage-Output 8-/10-Bit DACs, pp.1-28, (2008)

[12] MICROCHIP : Charge Pump DC-TO-DC Voltage Converter, pp.1-10, (2001)

[13] TEXAS INSTRUMENTS : Qudruple Differential Line Receivers, pp.1-9, (2006)

APPENDIX A. DD MOTOR

Tble.1 shows details of the servo motor SGMCS-02B type.

Table. 1 servo motor rating and specific

Voltage	200V	
Servo motor type	SGMCS-02B	
Rated output	W	42
Rated torque	N・m	2.00
Maximum torque	N・m	6.00
Stall torque	N・m	2.03
Rated current	A	1.9
Maximum current	A	5.4
Rated speed of rotation	min^{-1}	200
Maximum rotation speed	min^{-1}	500
Torque constant	Nm/A	1.28
Rotator inertia moment	$kg \cdot m^2 \cdot 10^{-4}$	25.0
Rated power rate	KW/s	1.60
Rated angle velocity	rad/s^2	800

APPENDIX B. THE PERFORMANCE OF dsPIC30F4011

Fig.29 shows the pin configuration of dsPIC30F4011. The signature of dsPIC30F4011 are shown in Table.2.

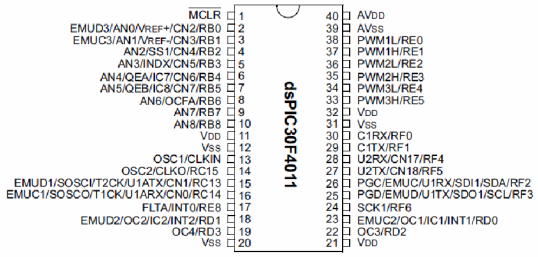

Fig. 29 Pins configuration of dsPIC30F4011

Table. 2 The signature of dsPIC30F4011

Pin number	40
Program memory(kB)	48
SRAM(bite)	2048
Timer number	5
I/O Pin	30
Orthogonal encoder	Exist

APPENDIX C. The parameter of the handling machine

Table.3 shows the parameter of the handling machine.

Table. 3 the parameter of the handling machine

parameter	name	value
m_1	mass of link1	0.165[kg]
m_2	mass of link2	0.07[kg]
m_3	mass of link3	0.085[kg]
l_1	length from edge of link1 to center	0.043[m]
l_2	length from edge of link2 to center	0.040[m]
l_3	length from edge of link3 to center	0.11[m]
M	mass of balancer	0.88[kg]
L	length from edge of balancer to center	0.046[m]
c	the viscous friction coefficient of shaft	0.001333[kgm^2/s]
J	inertia moment of motor	0.0025[kgm^2]
θ_0	Angle between link1 and link2	$\pi/4$[rad]
g	acceleration of gravity	9.8[m/s^2]

APPENDIX D. CONTROLLABLE

The controllable is sure if system can control to target. The observable is sure if system can know the state from input and output. These are important to design control systems. Define state equation as

$$\dot{x} = Ax(t) + Bu, \tag{50}$$
$$y = Cx(t). \tag{51}$$

In eq.(50), if control input $u(t)$ can take finite-time t_f to shift from arbitrary initial state x_0 to state of hope x_f, eq.(50) is defined as controllable.
If controllable matrix U_c has rank n, the system is necessary and sufficient condition for comfortable. It shows

$$U_c = [B,\, AB,\, A^2B, \cdots,\, A^{n-1}B], \tag{52}$$
$$\mathrm{rank}U_c = n. \tag{53}$$

In this paper,

$$U_c = [B,\, AB] = \begin{bmatrix} 0 & \frac{1}{a} \\ \frac{1}{a} & -\frac{c}{a^2} \end{bmatrix}, \tag{54}$$
$$|U_c| = -612.69(\neq 0), \tag{55}$$
$$\mathrm{rank}(U_c) = 2. \tag{56}$$

A is matrix(2×2), eq.(56) corresponds with eq.(53), so eq.(50) is comfortable system.

APPENDIX E. THE OPTIMAL REGULATOR

The performance index shows

$$J = \int_0^\infty [x^T Q x + u^T R u] dt. \tag{57}$$

$Q(3 \times 3)$ and $R(1 \times 1)$ are weighting matrixes. Q is positive-semi definite, R is positive definite. Control input u is decided, when J is minimum. The performance index J minimization reduces the consumption energy and improves transient property. When J of eq. (56) is minimized, the optimal feedback control input U^0 shows

$$U^0 = -Kx = -R^{-1}B^T P x. \tag{58}$$

U^0 is uniquely decided, and then minimum value is,

$$\min J = x^T(0) P x(0). \tag{59}$$

P is the symmetric matrix. It is decided as the only positive definite in Riccati type matrix which shows as follows:

$$A^T P + PA + Q - PBR^{-1}B^T P = 0. \tag{60}$$

APPENDIX F. ENCODER

Fig.30 shows the relations of encoder.

When phase A is early to phase B, the motor is judged to rotate a positive direction. When phase A is late to phase B. It is judged to rotate a negative direction.

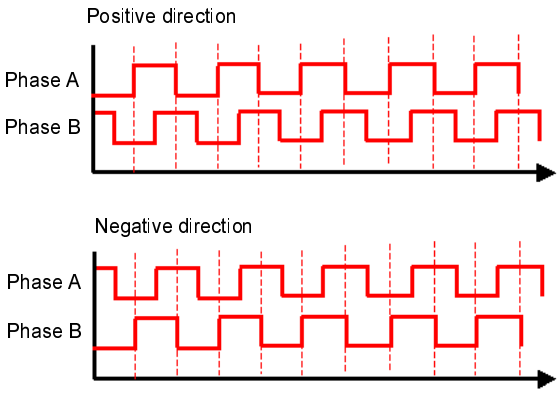

Fig. 30 Phase$A$ and phase$B$

APPENDIX G. PHERIPHERALS

G.1 Line Receiver

Fig.31 has shown the pins configuration of the line receiver[13]. Fig.31 means that when output of the encoder phase$A$ is input into pin2, phase$\bar{A}$ is input into pin1, and difference of voltages between them is output into pin3. Phase B is similar. Therefore, 4 phases can be used as encoder.

G.2 DA Converter

Fig.32 shows the block diagram of DA converter[11], Fig.33 shows the pins configuration of DA converter.

In Fig.32, 10bits data of DB0∼DB9 are input and latched as a WR signal. Some data is pass along from input register to DAC register by DAC signal, they are

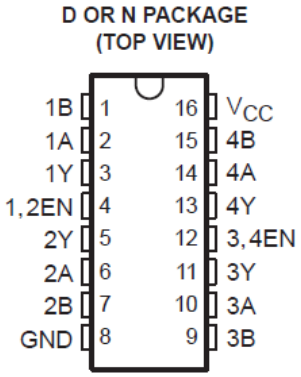

Fig. 31 The pins configuration of the line reciever

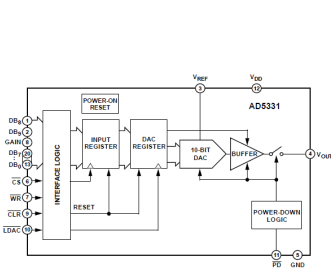

Fig. 32 The block diagram of the DA converter

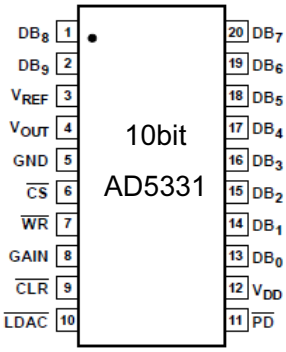

Fig. 33 The pins configuration of the DA converter

output 10bits of DAC as an analog signal, and V_{OUT} is output via the buffer amplifier. GAIN pin of Fig.33 can be set up 1 time or twice. In this paper, it is used twice.

G.3 Differential Operation Amplification

The operation amplification was used to convert output value 0∼1023 of DA converter into a negative value. Fig.34 shows the circuit diagram which is included the differential operation amplification. The capacitor which is connected parallel to R_4 is the role of the low pass filter.

The voltage of the negative terminal is shown as follows:

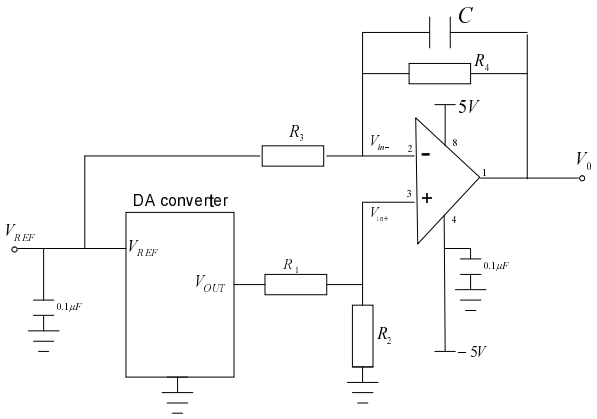

Fig. 34 The circuit diagram which is included an operation amplification

$$\frac{V_{REF} - V_{in-}}{R_3} = \frac{V_{in-} - V_0}{R_4},$$
$$V_{in-} = \frac{R_4 V_{REF} + R_3 V_0}{R_3 + R_4}. \quad (61)$$

The voltage of the positive terminal is shown as follows:

$$V_{in+} = \frac{R_2}{R_1 + R_2} V_{OUT}. \quad (62)$$

A virtual short-circuit is realized,

$$V_{in-} = V_{in+}, \quad (63)$$
$$\frac{R_4 V_{REF} + R_3 V_0}{R_3 + R_4} = \frac{R_2}{R_1 + R_2} V_{OUT}, \quad (64)$$
$$\frac{R_3}{R_3 + R_4} V_0 = \frac{R_2}{R_1 + R_2} V_{OUT} - \frac{R_4}{R_3 + R_4} V_{REF}. \quad (65)$$

Here, $R_1 = R_3$ and $R_2 = R_4$

$$R_1 V_0 = R_2 V_{OUT} - R_2 V_{REF}, \quad (66)$$
$$V_0 = \frac{R_2}{R_1}(V_{OUT} - V_{REF}). \quad (67)$$

The resistance ratio is denoted in eq.(68), and V_{OUT} is denoted eq.(69), when the gain of DA converter is 2. Here, D is decimal number 0〜1023.

$$R_1 : R_2 = R_3 : R_4 = 1 : 2, \quad (68)$$
$$V_{OUT} = 2 V_{REF} \frac{D}{2^{10}}. \quad (69)$$

By substituting the eqs. (68) and (69) into (67), we obtain

$$V_0 = 2(2 V_{REF} \frac{D}{2^{10}} - V_{REF}). \quad (70)$$

Here, V_{REF} is 2.5[V]. Then,

$$D = 1023 \Rightarrow V_0 \fallingdotseq 5[V], \quad (71)$$
$$D = 0 \Rightarrow V_0 = -5[V], \quad (72)$$
$$D = 512 \Rightarrow V_0 = 0[V]. \quad (73)$$

It is given −5V〜5V.

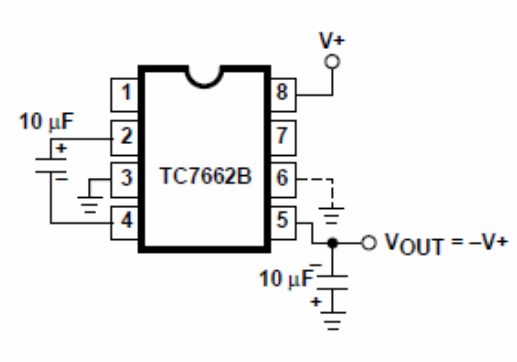

Fig. 35 The connection of DC — DC converter

G.4 DC-DC Converter

Fig.35 shows the connection of DC — DC converter[12].

When 5[V] is input to the 8 pin, −5[V] is output in 5 pin only by using two capacitors of 10 µ F. This is used as a negative voltage supply in the operation amplification.